Imaging the Moisture-Induced Degradation Process of 2D Organolead Halide Perovskites

Jianbo Tang, Wenming Tian,* Chunyi Zhao, Qi Sun, Chunyang Zhang, Hui Cheng, Yantao Shi, and Shengye Jin*

Cite This: *ACS Omega* 2022, 7, 10365−10371

Read Online

ACCESS | Metrics & More | Article Recommendations | Supporting Information

ABSTRACT: Two-dimensional (2D) and quasi-2D Ruddlesden−Popper (RP) phase organolead halide perovskites are promising materials for both photovoltaic and optoelectronic devices. Although they are known to be more stable when exposed to moisture than their 3D counterpart, chemical degradation of these materials under moisture, which not only leads to a significant drop in device performance but also leads to lead leakage, yet remains one of the most serious hurdles for their practical applications. To gain insight into the degradation mechanism of 2D/quasi-2D perovskites under moisture conditions, the degradation pathway of 2D/quasi-2D $(PEA)_2(MA)_{n-1}Pb_nI_{3n+1}$ (PEA = $C_6H_5C_2H_4NH_3^+$, MA = $CH_3NH_3^+$, and n is the number of perovskite layers between adjacent organic spacer layers) perovskite single crystals (SCs) and thin film are explored. We observe the degradation process by mapping the photoluminescence of the 2D perovskites and demonstrate that the larger-n phases all directly degrade into the relative stable $n = 1$ phase and MAI and PbI_2, which is a mechanism different from that in previous reports and further confirmed in the 2D perovskite thin film. This degradation process is also found to be independent of the boundary and morphology of the SCs. This discovery provides a new perspective for understanding the chemical degradation of the 2D perovskite materials and may inspire new solutions for improving their moisture stability.
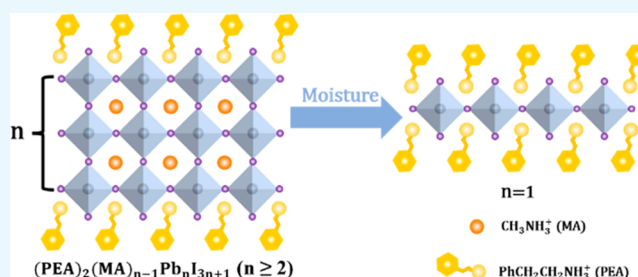
INTRODUCTION

Lead halide perovskites have great potential in the fields of solar cells, light-emitting diodes (LEDs), photodetectors, and optical gain materials.[1−8] Conventional three-dimensional (3D) methylammonium lead iodide perovskite have the advantages of suitable band gap width, large absorption coefficient, high photoluminescence quantum yield, high charge carrier mobility, long carrier lifetime, and diffusion length.[1,9−17] Despite these outstanding properties, the instability of 3D perovskite to moisture, light, and oxygen severely limit its further applications.[18−21] In recent years, the RP phase 2D/quasi-2D perovskites have attracted much attention for their higher resistance to moisture than conventional 3D perovskites.[22−27] The structural formula of 2D perovskites is $A_2B_{n-1}M_nX_{3n+1}$, where A is a long-chain aliphatic or aromatic alkylammonium cation that acts as a spacer layer between the perovskite layers, B is an organic cation, M is a divalent metal cation, X is the halide. The integer n is the number of perovskite layers between adjacent organic spacer layers.[2,28,29] It is reported that by converting the upper surface of the 3D perovskite into a (quasi-) 2D perovskite layer, both the efficiency and stability of the perovskite photovoltaics are improved by lower surface defect density and enhanced moisture stability.[30] Solar cells based on 2D/quasi-2D perovskites exhibit remarkably long-term stability by

blocking the moisture penetration pathway from the external atmosphere to the inner perovskite film.[31] Meanwhile, other observations for the high stability of the 2D/quasi-2D perovskite materials and solar cells have also been reported.[22,23,32−34]

To maximize its applications, researchers explore the reasons for their enhanced stability by probing the degradation chemistry under moisture environments. So far, much effort has been put into exploring the degradation process of 2D/quasi-2D perovskites.[31,35] Compared with 3D perovskite, the degradation pathway of 2D perovskite is completely different due to the introduction of hydrophobic cation such as n-butylammonium (BA) and phenylethylammonium (PEA). Previous reports showed that the improved moisture stability of quasi-2D perovskites is attributed to a disproportionation degradation mechanism, leading to the formation of the small-n surface protection layer that effectively protects the materials from further degradation.[31] Wygant et al. proposed that larger-

n phase degrades into $(n-1)$ phase and 3D MAPbI$_3$ upon exposure to moisture in 2D perovskite thin film, and they also demonstrated that the dynamic growth of micrometer-scale crystallites and cracks at the surface of quasi-2D perovskite film during degradation, which is proposed as byproducts of the disproportionation mechanism.[35] The results are consistent with density functional theory calculations that the formation energy increases as the value of n decreases, indicating the improved stability of small-n species.[32]

Compared with 2D perovskite thin film with complex phases, pure-phase 2D perovskite single crystal (SC) is a better model system for clarifying the degradation mechanism of 2D/quasi-2D perovskites. To our knowledge, no relevant research on the degradation chemistry of 2D perovskite SCs has been reported. In this work, we directly observe the degradation process of $(PEA)_2(MA)_{n-1}Pb_nI_{3n+1}$ 2D perovskite SCs with different n values and 2D perovskite thin film under moisture conditions by using a laser-scanned PL imaging microscopy coupled with time-correlated single photon counting (TCSPC) module. By collecting the PL spectra and images of 2D perovskites under moisture conditions (~85% relative humidity), we spatially observe the degradation process of the micron-scale SC and demonstrate that the larger n phases degrade into the relative stable $n = 1$ phase and MAI and PbI$_2$, which is different from the observed disproportionation mechanism that larger n phase degrades into $(n-1)$ phase and 3D MAPbI$_3$. We also discovered that the degradation process of SCs is independent of the boundary and morphology of the crystals. This degradation process was further confirmed in the 2D perovskite thin film. This work systematically examines the moisture-induced degradation principles of both 2D/quasi-2D perovskite single crystals and thin films, which broadens the understanding of the chemical change to these kinds of 2D materials under moisture.

■ RESULTS AND DISCUSSION

We synthesize the $(PEA)_2(MA)_{n-1}Pb_nI_{3n+1}$ layered 2D perovskite single crystals (SCs) with $n = 1-3$ according to the reported method described in the Supporting Information.[36] The crystal structure is schematically demonstrated in Figure 1a and is confirmed by XRD patterns (Figure 1b) which
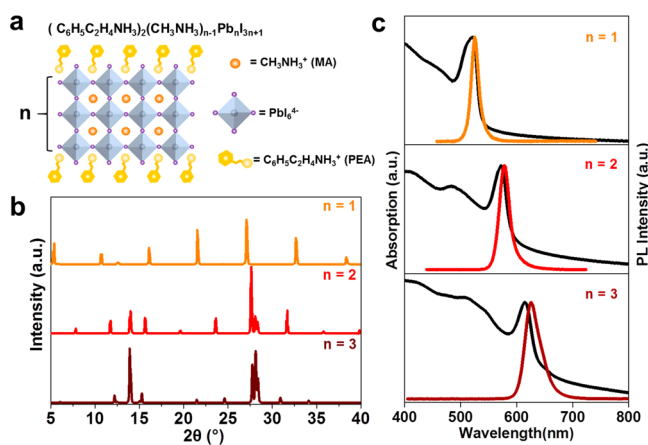
Figure 1. Spectroscopic and structure characterizations of 2D perovskite crystals. (a) Schematic of crystal structure of $(PEA)_2(MA)_{n-1}Pb_nI_{3n+1}$ 2D perovskites. (b) XRD patterns of pristine 2D perovskites with $n = 1-3$. (c) UV–vis absorption and PL spectra of $(PEA)_2(MA)_{n-1}Pb_nI_{3n+1}$ 2D perovskites with $n = 1-3$.

indicates that the 2D SCs are phase-pure and exhibit excellent crystallinity in ensemble. Figure 1c shows the UV−vis absorption and PL spectra of $(PEA)_2(MA)_{n-1}Pb_nI_{3n+1}$ SCs with $n = 1-3$. Because of the quantum confinement effect, the optical bandgap of the 2D perovskite SCs decreases from ~2.38 eV for $n = 1$ to ~1.98 eV for $n = 3$. Both UV−vis absorption and PL spectra further confirm the phase purity of the 2D perovskite SCs. The SEM images of typical exfoliated SCs of $n = 1-3$ are shown in Figure S1, which show a clear layered structure.

The 2D perovskite SCs are mechanically exfoliated with scotch tape with a lateral dimension of tens of micrometers and a thickness of a few hundred nanometers. We perform the photoluminescence (PL) imaging measurement of individual 2D perovskite SCs placed at a chamber with ~85% relative humidity (RH) by using a laser-scanned PL imaging microscopy coupled with time-correlated single photon counting (TCSPC). In previous works, different humidity levels are selected to explore the degradation chemistry of perovskite materials, indicating the degradation mechanism is unaffected within this humidity range.[24,31,32,35,37−42] Therefore, we selected 85% RH, which is within the range of humidity used in previous works. The setup of the constant humidity reaction chamber and the laser-scanned PL imaging microscopy are shown in Figures S2 and S3. A set of optical images and PL variation of a typical $n = 2$ perovskite SC as a function of time under moisture conditions are shown in Figure 2.
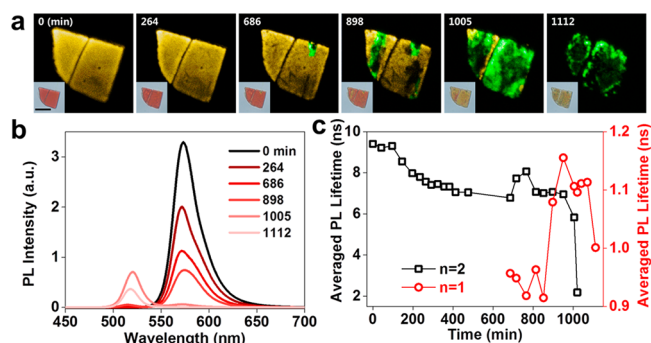
Figure 2. Microscopic PL and spectroscopic characterization of degradation of an exfoliated individual 2D $(PEA)_2MAPb_2I_7$ perovskite SC ($n = 2$) under moisture conditions. (a) A set of the laser-scanned confocal PL intensity images collected in the emission channels of 570−590 nm (yellow) and 515−535 nm (green), showing the evolution of the degradation process under different exposure time. The insets are the optical images. The scale bar is 10 μm. (b) Variation of PL spectra of the same 2D perovskite crystal ($n = 2$) at different exposure times. (c) Variation of the average PL lifetime as a function of exposure time extracted from TRPL kinetics of the $n = 2$ and newly generated $n = 1$ phase.

In Figure 2a, the optical and PL intensity images of the $(PEA)_2MAPb_2I_7$ ($n = 2$) SC are clear and homogeneous at the initial time. Upon exposure to moisture, the SC surface distinctly becomes rough, and the PL intensity decreases because of the degradation of the material. After 686 min (11.4 h) of exposure, it is obvious that the crystal begins to crack and part of the crystal starts to turn yellow, accompanied by a further decrease of PL intensity. In Figure 2b, in addition to the observed intrinsic PL of $n = 2$ perovskite SC with a central wavelength of ~575 nm, a new emission peak centered at

~520 nm appears, which agrees with the excitonic feature of n = 1 perovskite phase (Figure 1c) and was also confirmed in previous works to be the n = 1 phase generated during degradation.[31,35] Furthermore, we also excluded the PbI_2 (nonperovskite product of degradation) emission at ~520 nm by collecting the emission from PbI_2 film under the same experimental conditions, because the PbI_2 is a nonfluorescent phase under such low excitation intensity (Figure S4). This observation is also consistent with the PL images shown in Figure 2a, showing that PL of n = 1 (degraded from large n) only appears at the local sites where the crystal turns yellow in the optical image and the PL of n = 2 perovskite disappears. This observation clearly demonstrates the degradation of n = 2 to n = 1 perovskite phase under moisture conditions. After 1112 min (~18.5 h) of exposure, the intrinsic n = 2 perovskite phase almost completely degrades and the generated n = 1 phase continues to decompose quickly in the meanwhile to nonfluorescent species (PbI_2 and PEAI) (Figure 2a,b). Apparently, heterogeneous degradation locations and rates are observed during degradation from n = 2 to n = 1, which may relate to variations of the local crystalline quality, and this microstructural heterogeneity of the degradation process does not affect the degradation mechanism.

To better understand the changes in photophysical properties during the degradation process, the time-resolved PL kinetics (TRPL) of the pristine n = 2 and the newly generated n = 1 phase at various exposure times are obtained with representative PL kinetics shown in Figure S5b,c. The data were well fitted by the following multiexponential function of $I(t) = \sum A_i \exp(-t/\tau_i)$ (i = 1, 2, and 3), where A_i is the amplitude of each component, and τ_i is the corresponding lifetime. The average PL lifetime is calculated as $\tau_{Ave} = \sum A_i \tau_i / \sum A_i$. However, it is difficult for us to give a specific origin of each component. We just give a qualitative determination by the variation of the average PL lifetime to illustrate the processes that the SCs may undergo during degradation under humidity conditions. Figure 2c shows the evolution of the average PL lifetime of the pristine n = 2 and the newly generated n = 1 phase under moisture. The average PL lifetime of n = 2 phase decreases as exposure time increases and is consistent with the evolution of PL intensity (Figure S6b), which is attributed to increased nonradiative recombination caused by the invasion of moisture during degradation. At longer exposure time, the average PL lifetime of n = 2 phase exhibits a sharp decrease at exposure time >900 min, indicating the degradation process is not homogeneous and accelerates under more moisture. In addition, the PL lifetime of the newly generated n = 1 phase slightly increases possibly due to the passivation effect of moisture, and then it decreases upon further exposure which is also due to the increased non-radiative recombination caused by moisture. Comparison of the decay rates of n = 2 and newly generated n = 1 phase at longer exposure time indicates that the rapid degradation of the n = 2 phase under moisture coincides with the generation and surface passivation process of the n = 1 phase.

In previous reports, Yan et al. demonstrated that larger-n members tend to disproportionate to n = 3 and n = ∞ members in some oxide RP perovskites.[43] Stoumpos et al. proposed a stabilizing disproportionation mechanism to explain the higher stability of 2D organolead halide perovskite over their 3D counterpart.[22] Further, Wygant et al. verified the mechanism on both $(nBA)_2(MA)_{n-1}Pb_nI_{3n+1}$ bare film and solar cell devices by using PL, ToF-SIMS, and other

characterization methods.[31] They described the disproportionation process as

$$(nBA)_2(MA)_3Pb_4I_{13} (n = 4) \xrightarrow{H_2O} (nBA)_2(MA)_2Pb_3I_{10} (n = 3)$$
$$+ MAPbI_3 (n = \infty)$$
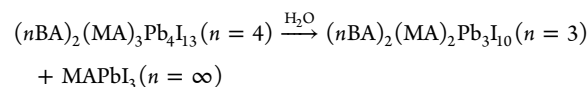
By using the PL imaging technique, this work directly observes the degradation pathway from n = 2 to n = 1 in individual quasi-2D perovskite SC and demonstrates that the degradation occurs randomly and has no relation to the crystal boundary or shape. Previous density functional theory calculation of PEA-MAPI perovskites with different n values demonstrates that the formation energy decreases as the n value increases, indicating the small-n phase is the thermodynamically stable phase.[32] The calculation result is consistent with our and previous work.[22,31,35] However, different from the disproportionation mechanism, we did not obtain the PL of $MAPbI_3$ in the long-wavelength region near 778 nm; thus, we deduce that MAI and PbI_2 were generated by direct decomposition of $MAPbI_3$. We further verify this process in 2D perovskite SCs with different n values.

In Figure 3, we select a typical n = 3 perovskite SC to further explore the degradation mechanism. The optical and PL
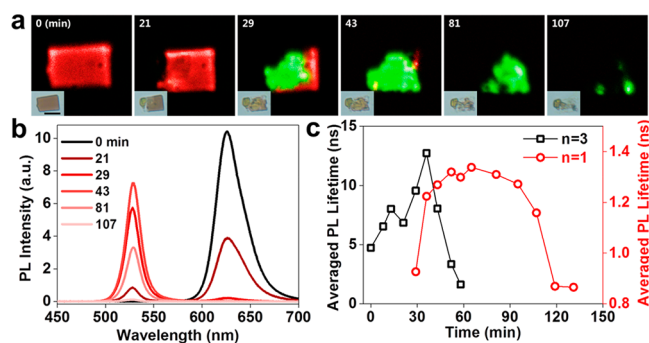

Figure 3. Microscopic PL and spectroscopic characterization of degradation of an exfoliated individual 2D $(PEA)_2MA_2Pb_3I_{10}$ perovskite crystal (n = 3) under moisture conditions. (a) A set of the laser-scanned confocal PL intensity images collected in the emission channels of 600−640 nm (red) and 490−550 nm (green), showing the evolution of the degradation process under different exposure times. The insets are the optical images. The scale bar is 5 μm. (b) Variation of PL spectra of the same 2D perovskite crystal (n = 3) at different exposure time. (c) Variation of the average PL lifetime as a function of exposure time extracted from TRPL kinetics of the n = 3 and newly generated n = 1 phase.

intensity images of the crystal as a function of exposure time are shown in Figure 3a. At an exposure time of 21 min, the crystal apparently starts to degrade from the left corner of the crystal. In Figure 3b, PL centered at 625 nm is the intrinsic emission of the n = 3 perovskite phase, and the intensity declines sharply in the first ~20 min. Meanwhile, no peak shift caused by moisture is observed at different exposure time in the n = 3 and n = 1, 2 phases (Figure S7c). As the exposure time increases, the sharp emission peak centered at ~520 nm gradually appears, which coincides with the excitonic feature of n = 1 $(PEA)_2PbI_4$ perovskite.[44] The PL intensity increases until it reaches a maximum at 43 min of exposure time. This result is also consistent with the PL intensity images shown in Figure 3a. The variation of PL intensity for the two species is shown in Figure S6c. It should be noted that the degradation time is determined by size, thickness, local defects, moisture resistance

of the materials, and other possible reasons such as cracks on the crystal surface. Therefore, it is inadequate to compare the stability of the $n = 2$ and $n = 3$ perovskite SC with different conditions. In addition to a longer PL lifetime of $n = 2$ SC which represents fewer trap states, the size of the $n = 2$ SC in Figure 2 is much larger than that of the $n = 3$ SC in Figure 3, which may also lead to a longer degradation time of $n = 2$ SC.

Similar to the degradation process of $n = 2$ SC phase, the PL of $n = 1$ phase appears where the PL of $n = 3$ phase decreases significantly, indicating a direct degradation from $n = 3$ to $n = 1$ phase. TRPL of $n = 3$ phase and newly generated $n = 1$ phase as a function of exposure time are exhibited in Figure 3c. The average PL lifetime of the $n = 3$ phase increases in the beginning probably due to the passivation effect of water molecules and then decreases as the exposure time increases. The average PL lifetime of the newly generated $n = 1$ phase exhibits a similar trend with $n = 1$ phase degraded from $n = 2$ SC, including sequential generation, passivation, and degradation steps. The variation of average PL lifetime is the result of the combined effect of passivation, increased density of trap states, and degradation. As mentioned above in the case of $n = 2$ SC, we did not detect PL of 3D MAPbI$_3$ during degradation in $n = 3$ SC, suggesting that the degradation mechanism is the same as that in $n = 2$ and 3 SCs, which is different from the reported disproportionation mechanism.[31] Moreover, instead of observing the continuous reduction process from n to (n-1) phase during degradation, we only obtain $n = 1$ phase, indicating $n = 1$ perovskite phase is an important transition state in 2D perovskite degradation, which is consistent with the DFT calculation that the small-n phases are more stable.[32] Additionally, the decomposition of $n = 1$ SC was also explored (Figure S8), which shows a direct decomposition from $n = 1$ phase to nonperovskite phase. On the basis of the results above, we speculate the following degradation mechanism in SCs:

$$(PEA)_2(MA)_{n-1}Pb_nI_{3n+1}$$
$$\xrightarrow{H_2O} (PEA)_2PbI_4 + (n-1)MAI + (n-1)PbI_2 \, (n \geq 2)$$
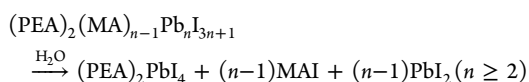
In order to further confirm the above degradation mechanism, we explore the degradation pathway of quasi-2D $(PEA)_2(MA)_{n-1}Pb_nI_{3n+1}$ perovskite thin film prepared as $n = 4$ under moisture conditions. The Optical image in Figure S9a and SEM image in Figure S10 shows the flat surface of the as-prepared film, which indicates the high quality of the film. Before moisture treatment, PL spectra were obtained under both back and front excitation as shown in Figure S11. Upon front-excitation, the 2D perovskite film exhibits strong PL emission centered at 735 nm, corresponding to the large-n phase of $(PEA)_2(MA)_{n-1}Pb_nI_{3n+1}$ perovskites. Upon back-excitation, besides the strong emission peak centered at 735 nm, a few small peaks at higher energies which correspond to $n = 2, 3,$ and 4 phase of $(PEA)_2(MA)_{n-1}Pb_nI_{3n+1}$ perovskites appear, implying that the small-n phases located at the bottom surface and the large-n phases located at the upper surface of the film, which is consistent with previously reported 2D perovskite thin film.[45] Figure 4a shows the PL evolution of 2D perovskite thin film under moisture. As exposure time increases, emission peak at 735 nm becomes weaker, suggesting degradation of large-n phase. At exposure time of 122 h, a sharp and strong PL peak located at ~520 nm appears, which indicates the degradation of inner small-n phases into the relative water-resistant $n = 1$ phase. At an exposure time of
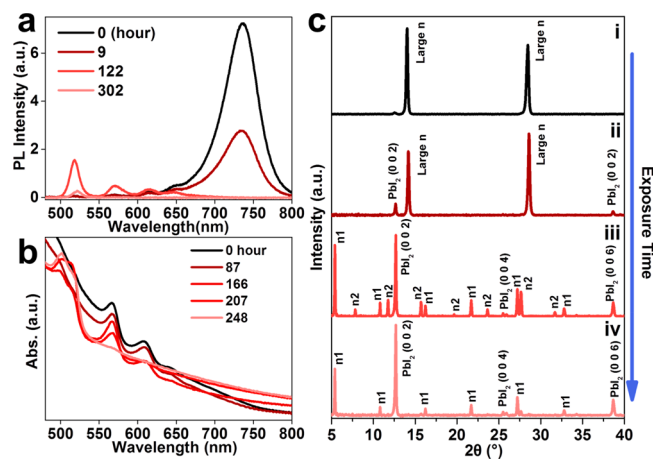

Figure 4. Spectroscopic and structural characterization of degradation of 2D $(PEA)_2MA_{n-1}Pb_nI_{3n+1}$ perovskite thin film prepared as $n = 4$ under moisture conditions. (a) Variation of PL spectra of the 2D perovskite thin film at different exposure times. (b) Variation of UV−vis absorption spectra under different exposure time. (c) Evolution of XRD patterns from the same $(PEA)_2MA_{n-1}Pb_nI_{3n+1}$ thin film ($n = 4$) during degradation. The blue arrow indicates the evolution direction.

302 h, the film apparently degraded into many small particle-like surface structures (Figure S9b) accompanied by a decrease in the PL intensity of the $n = 1$ phase. The small particle-like surface structures are similar to those observed by Wygant et al. for nBA-MAPbI$_3$ film after 72 h exposure to RH 78%, which is attributed to small-n perovskite.[35] To confirm the particle-like structures, we performed steady-state PL spectra and PL imaging measurements (Figure S9c) and confirmed that the particle-like structures are $n = 1$ perovskite phase, which is consistent with the degradation mechanism.

Meanwhile, the evolution of UV−vis absorption spectra of the 2D perovskite thin film under moisture conditions is shown in Figure 4b. Apart from the lowest bandgap absorption, three absorption peaks located at ~567 nm (2.19 eV), ~608 nm (2.04 eV), and ~640 nm (1.94 eV), which respectively represent $n = 2$, $n = 3$, and $n = 4$ perovskite phase are present before reaction, which is consistent with the PL spectra in Figure S11. After exposure to moisture, the intensity of the absorption peaks of the quasi-2D perovskite phases decreases, and finally, only the absorption peaks of the $n = 1$ perovskite phase (Figure 1c) and nonperovskite phase PbI$_2$ (Figure S4) are observed, indicating the destruction of large-n lattice and generation of $n = 1$ phase, which is consistent with the evolution of PL spectra in Figure 4a. In order to investigate the structural changes under moisture, X-ray diffraction (XRD) measurements were also performed. As shown in Figure 4c, the as-prepared 2D perovskite thin film shows two strong peaks located at $2\theta \approx 14°$ and $2\theta \approx 28°$, which correspond to (111) and (202) planes of large-n phases located at the upper surface of the 2D perovskite film.[31,45] After long time exposure to moisture, the XRD pattern includes both perovskite phases with different n values and nonperovskite phase PbI$_2$ due to degradation. Finally, the 2D perovskite phase with $n \geq 2$ all degrade into $n = 1$ phase.

This observation is consistent with the degradation process of $n = 2$ and 3 SCs as exhibited in Figures 2 and 3, which further validates our proposed degradation mechanism. This degradation pathway unravels the relatively high humidity stability of the $n = 1$ 2D perovskite, where the large-n and

small-n phases all degrade into $n = 1$ phase. Similar to the hydration-driven degradation mechanism for 3D MAPbI$_3$ perovskite, the dissociation of highly volatile and water-soluble methylammonium cation leads to the instability of the quasi-2D phase due to strong hydrogen bonds formed through ready interaction between methylammonium and water.[19,46,47] These provide promising ways to further improve the moisture stability of quasi-2D perovskites, such as replacing the methylammonium cation or introducing more aliphatic or aromatic alkylammonium spacer with more hydrophobic groups.

■ CONCLUSION

In summary, by using the laser-scanned PL imaging microscopy, we directly observed the degradation process of 2D/quasi-2D perovskite $(PEA)_2(MA)_{n-1}Pb_nI_{3n+1}$ SCs ($n = 1-3$) and thin film ($n = 4$) under moisture conditions. We find that the degradation process occurs randomly in the 2D perovskite SCs and has no relation to the crystal boundary and morphology. Different from the reported degradation mechanism of 2D perovskites that larger-n phase degrade into ($n-1$) phase and 3D MAPbI$_3$, we demonstrated the degradation of the larger-n phase into the relatively stable $n = 1$ phase and MAI and PbI$_2$ by directly observing the generation of $n = 1$ phase exactly where the larger-n phases degrade. This discovery of the quasi-2D perovskite degradation pathway may help to find new methods to significantly enhance the stability of 2D/quasi-2D perovskites against moisture.

■ EXPERIMENTAL SECTION

Synthesis of CH$_3$NH$_3$I. The CH$_3$NH$_3$I was synthesized by mixing 61 mL of methylamine (33 wt % in absolute ethanol) and 65 mL of HI (57 wt % in water by weight) in a flask in an ice bath at 0 °C for 2 h with stirring. The methylammonium iodide (CH$_3$NH$_3$I) was achieved as the solvent was carefully removed using a rotate evaporator (Dragon Laboratory Instruments Limited RE100-PRO, China) at 50 °C. The white CH$_3$NH$_3$I powder was washed with diethyl ether three times. The final product was collected by filtration and dried at 80 °C in a vacuum oven for 24 h.

Synthesis of the PEA$_2$(MA)$_{n-1}$Pb$_n$I$_{3n+1}$ 2D Perovskite SCs. PEA$_2$PbI$_4$ ($n = 1$). PbI$_2$ (46.1 mg, 0.1 mmol) and PEAI (24.5 mg, 0.1 mmol) were dissolved in about 4 mL of HI (57 wt % in H$_2$O) by stirring and heating to 130 °C. The plate-like SCs were obtained after the solution was cooled down to room temperature (~10 °C/30 min). Then the SCs were washed with diethyl ether and dried at 60 °C under vacuum for 24 h before use.

PEA$_2$(MA)Pb$_2$I$_7$ ($n = 2$). PbI$_2$ (184.4 mg, 0.4 mmol), MAI (106.53 mg, 0.67 mmol), and PEAI (41.7 mg, 0.17 mmol) were dissolved in about 2 mL of HI (57 wt % in H$_2$O) by stirring and heating to 130 °C. The subsequent steps were carried out in a similar way to what was described in PEA$_2$PbI$_4$ ($n = 1$).

PEA$_2$(MA)$_2$Pb$_3$I$_{10}$ ($n = 3$). PbI$_2$ (184.4 mg, 0.4 mmol), MAI (106.53 mg, 0.67 mmol), and PEAI (16.7 mg, 0.067 mmol) were dissolved in about 2 mL of HI (57 wt % in H$_2$O) by stirring and heating to 130 °C. The subsequent steps were carried out similarly as already described.

Preparation of Multilayered 2D Perovskite Thin Films. Glass substrates were cleaned via ultrasonication in isopropyl alcohol, distilled water, and acetone in turn followed

by 20 min oxygen plasma. The precursor solution of $(PEA)_2(MA)_{n-1}Pb_nI_{3n+1}$ ($n = 4$) was prepared by dissolving PEAI, MAI, and PbI$_2$ with a stoichiometric ration of 2:3:4 in anhydrous DMF with a total Pb^{2+} concentration of 0.6 M. Before film fabrication, an ultrasonication bath was used to help the solute dissolve to reach a clarified solution. For the hot-casting, the rinsed glass substrates were first preheated to 100 °C on a hot plate for 10 min right before spin-coating. The hot substrates were immediately transferred to spin-coated platform (at room temperature) followed by dropping 50 μL precursor solution onto the hot glass substrates. The spin speed is 5000 rpm, and the acceleration is 1500 rpm/s. The film turned brown several seconds after the beginning of spin-coating. The total spin-coating time is 50 s. After that, the film was annealed at 100 °C for 5 min.

Preparation of PbI$_2$ Thin Films. The PbI$_2$ thin films were prepared in the same way as the multilayered 2D perovskite thin films, but the precursor solution was only PbI$_2$ at a concentration of 0.6 M.

X-ray Diffraction Measurement on 2D Perovskite Films and SCs. The $(PEA)_2(MA)_{n-1}Pb_nI_{3n+1}$ ($n = 4$) multilayered 2D perovskite films and SCs with $n = 1-3$ were both measured by powder X-ray diffraction system (PXRD) (X'pert Pro-1, PANAlytical).

UV−vis Absorption Measurement. UV−vis absorption spectra were performed by UV−vis absorption spectrometer (Cary 60, Aglient Technologies). $(PEA)_2(MA)_{n-1}Pb_nI_{3n+1}$ ($n = 4$) thin films were taken out of the reaction chamber at different exposure time for the UV−vis spectra measurement. In order to measure the UV−vis absorption spectra of 2D perovskite SCs, the bulk 2D perovskite SCs were repeatedly exfoliated by scotch tape and transported to glass coverslips. Then the scotch tape was removed, and the exfoliated 2D layer crystals were left on the coverslip.

PL Measurement. The measurements were performed on a home-built laser-scanned imaging microscopy coupled with time-correlated single photon counting (TCSPC). The schematic was shown in Figure S3. The laser beam was focused on the sample through a 100× air objective lens (NA = 0.95, Olympus PLFLN 100×) at 450 nm wavelength (SC400-PP, Fianium, U.K.). Each PL intensity image obtained contains 256 × 256 pixels. The intensity of the laser source was adjusted by a neutral density filter and measured by a power meter (PM100D S1003VC, Thorlabs, U.S.A.). Two high speed detectors (HPM-100-40 and HPM-100-50, Hamamatsu, Japan) were used to collect fluorescence at different emission regions by using band-pass filters. The steady-state PL emission spectra were obtained by a monochromator (SpectraPro-HRS-300, Princeton Instruments, U.S.A.) coupled with a charge coupled device (CCD) camera (PIXIS 100, Princeton Instruments, U.S.A.), which shares the same microscope objective for signal collection with laser-scanned confocal PL imaging microscopy. To obtain PL spectra of the whole single crystal, we used a defocused 405 nm pulsed laser (PIXEA-405, Aurea technology, France) with a diameter of tens of micrometers, larger than the size of the single crystal.

Combination of the PL Intensity Images Collected from Different Emission Wavelengths in One SC. The combination of these two images is by superimposing PL image collected from short wavelength region with a transmittance of 50% onto the PL image collected from long wavelength region. The contrast and brightness are increased by 20% and 40%, respectively. All laser-scanned confocal PL

intensity images containing two different emission regions in this paper are processed in the same procedure.

ASSOCIATED CONTENT

Ⓢ Supporting Information

The Supporting Information is available free of charge at https://pubs.acs.org/doi/10.1021/acsomega.1c06989.

Figures S1−S11, SEM images, experimental setup, and additional results of measurements (PDF)

AUTHOR INFORMATION

Corresponding Authors

Shengye Jin − *State Key Laboratory of Molecular Reaction Dynamics and the Dynamic Research Center for Energy and Environmental Materials, Dalian Institute of Chemical Physics, Chinese Academy of Sciences, Dalian 116023, China;* ⓘ orcid.org/0000-0003-2001-2212; Email: sjin@dicp.ac.cn

Wenming Tian − *State Key Laboratory of Molecular Reaction Dynamics and the Dynamic Research Center for Energy and Environmental Materials, Dalian Institute of Chemical Physics, Chinese Academy of Sciences, Dalian 116023, China; Key Laboratory of Excited-State Materials of Zhejiang Province, Zhejiang University, Hangzhou 310027, China;* ⓘ orcid.org/0000-0003-0235-6652; Email: tianwm@dicp.ac.cn

Authors

Jianbo Tang − *State Key Laboratory of Molecular Reaction Dynamics and the Dynamic Research Center for Energy and Environmental Materials, Dalian Institute of Chemical Physics, Chinese Academy of Sciences, Dalian 116023, China; University of Chinese Academy of Sciences, Beijing 100049, China*

Chunyi Zhao − *Anhui Province Key Laboratory of Optoelectronic Material Science and Technology, School of Physics and Electronic Information, Anhui Normal University, Wuhu 241002, China*

Qi Sun − *MIIT Key Laboratory of Advanced Display Materials and Devices, Institute of Optoelectronics & Nanomaterials, College of Materials Science and Engineering, Nanjing University of Science and Technology, Nanjing 210094, China;* ⓘ orcid.org/0000-0002-7092-0705

Chunyang Zhang − *State Key Laboratory of Fine Chemicals, Department of Chemistry, School of Chemical Engineering, Dalian University of Technology, Dalian 116024, China*

Hui Cheng − *State Key Laboratory of Molecular Reaction Dynamics and the Dynamic Research Center for Energy and Environmental Materials, Dalian Institute of Chemical Physics, Chinese Academy of Sciences, Dalian 116023, China; Key Laboratory of Materials Modification by Laser, Ion and Electron Beams (Ministry of Education), School of Physics, School of Microelectronics, Dalian University of Technology, Dalian 116024, China*

Yantao Shi − *State Key Laboratory of Fine Chemicals, Department of Chemistry, School of Chemical Engineering, Dalian University of Technology, Dalian 116024, China;* ⓘ orcid.org/0000-0002-7318-2963

Complete contact information is available at:
https://pubs.acs.org/10.1021/acsomega.1c06989

Notes

The authors declare no competing financial interest.

REFERENCES

(1) Zhou, H.; Chen, Q.; Li, G.; Luo, S.; Song, T. B.; Duan, H. S.; Hong, Z.; You, J.; Liu, Y.; Yang, Y. Photovoltaics. Interface engineering of highly efficient perovskite solar cells. *Science* **2014**, *345*, 542−546.

(2) Cao, D. H.; Stoumpos, C. C.; Farha, O. K.; Hupp, J. T.; Kanatzidis, M. G. 2D Homologous Perovskites as Light-Absorbing Materials for Solar Cell Applications. *J. Am. Chem. Soc.* **2015**, *137*, 7843−7850.

(3) Zhang, W.; Eperon, G. E.; Snaith, H. J. Metal halide perovskites for energy applications. *Nat. Energy* **2016**, *1*, 16048−16055.

(4) Yuan, M.; Quan, L. N.; Comin, R.; Walters, G.; Sabatini, R.; Voznyy, O.; Hoogland, S.; Zhao, Y.; Beauregard, E. M.; Kanjanaboos, P.; Lu, Z.; Kim, D. H.; Sargent, E. H. Perovskite energy funnels for efficient light-emitting diodes. *Nat. Nanotechnol.* **2016**, *11*, 872−877.

(5) Li, G.; Rivarola, F. W.; Davis, N. J.; Bai, S.; Jellicoe, T. C.; de la Pena, F.; Hou, S.; Ducati, C.; Gao, F.; Friend, R. H.; Greenham, N. C.; Tan, Z. K. Highly Efficient Perovskite Nanocrystal Light-Emitting Diodes Enabled by a Universal Crosslinking Method. *Adv. Mater.* **2016**, *28*, 3528−3534.

(6) Dong, R.; Fang, Y.; Chae, J.; Dai, J.; Xiao, Z.; Dong, Q.; Yuan, Y.; Centrone, A.; Zeng, X. C.; Huang, J. High-gain and low-driving-voltage photodetectors based on organolead triiodide perovskites. *Adv. Mater.* **2015**, *27*, 1912−1918.

(7) Xing, G.; Mathews, N.; Lim, S. S.; Yantara, N.; Liu, X.; Sabba, D.; Gratzel, M.; Mhaisalkar, S.; Sum, T. C. Low-temperature solution-processed wavelength-tunable perovskites for lasing. *Nat. Mater.* **2014**, *13*, 476−480.

(8) Sutherland, B. R.; Sargent, E. H. Perovskite photonic sources. *Nat. Photonics* **2016**, *10*, 295−302.

(9) Im, J. H.; Jang, I. H.; Pellet, N.; Gratzel, M.; Park, N. G. Growth of $CH_3NH_3PbI_3$ cuboids with controlled size for high-efficiency perovskite solar cells. *Nat. Nanotechnol.* **2014**, *9*, 927−932.

(10) Baikie, T.; Fang, Y.; Kadro, J. M.; Schreyer, M.; Wei, F.; Mhaisalkar, S. G.; Graetzel, M.; White, T. J. Synthesis and crystal chemistry of the hybrid perovskite $(CH_3NH_3)PbI_3$ for solid-state sensitised solar cell applications. *J. Mater. Chem. A* **2013**, *1*, 5628−5641.

(11) De Wolf, S.; Holovsky, J.; Moon, S. J.; Loper, P.; Niesen, B.; Ledinsky, M.; Haug, F. J.; Yum, J. H.; Ballif, C. Organometallic Halide Perovskites: Sharp Optical Absorption Edge and Its Relation to Photovoltaic Performance. *J. Phys. Chem. Lett.* **2014**, *5*, 1035−1039.

(12) Yin, W. J.; Shi, T.; Yan, Y. Unique properties of halide perovskites as possible origins of the superior solar cell performance. *Adv. Mater.* **2014**, *26*, 4653−4658.

(13) Braly, I. L.; deQuilettes, D. W.; Pazos-Outón, L. M.; Burke, S.; Ziffer, M. E.; Ginger, D. S.; Hillhouse, H. W. Hybrid perovskite films approaching the radiative limit with over 90% photoluminescence quantum efficiency. *Nat. Photonics* **2018**, *12*, 355−361.

(14) Leijtens, T.; Stranks, S. D.; Eperon, G. E.; Lindblad, R.; Johansson, E. M. J.; McPherson, I. J.; Rensmo, H.; Ball, J. M.; Lee, M. M.; Snaith, H. J. Electronic Properties of Meso-Superstructured and Planar Organometal Halide Perovskite Films: Charge Trapping, Photodoping, and Carrier Mobility. *ACS Nano* **2014**, *8*, 7147−7155.

(15) deQuilettes, D. W.; Koch, S.; Burke, S.; Paranji, R. K.; Shropshire, A. J.; Ziffer, M. E.; Ginger, D. S. Photoluminescence Lifetimes Exceeding 8 μs and Quantum Yields Exceeding 30% in Hybrid Perovskite Thin Films by Ligand Passivation. *ACS Energy Lett.* **2016**, *1*, 438−444.

(16) D'Innocenzo, V.; Grancini, G.; Alcocer, M. J.; Kandada, A. R.; Stranks, S. D.; Lee, M. M.; Lanzani, G.; Snaith, H. J.; Petrozza, A. Excitons versus free charges in organo-lead tri-halide perovskites. *Nat. Commun.* **2014**, *5*, 3586−3591.

(17) Stranks, S. D.; Eperon, G. E.; Grancini, G.; Menelaou, C.; Alcocer, M. J. P.; Leijtens, T.; Herz, L. M.; Petrozza, A.; Snaith, H. J. Electron-Hole Diffusion Lengths Exceeding 1 Micrometer in an Organometal Trihalide Perovskite Absorber. *Science* **2013**, *342*, 341−344.

(18) Christians, J. A.; Miranda Herrera, P. A.; Kamat, P. V. Transformation of the excited state and photovoltaic efficiency of $CH_3NH_3PbI_3$ perovskite upon controlled exposure to humidified air. *J. Am. Chem. Soc.* **2015**, *137*, 1530−1538.

(19) Wang, D.; Wright, M.; Elumalai, N. K.; Uddin, A. Stability of perovskite solar cells. *Sol. Energy Mater. Sol. Cells* **2016**, *147*, 255−275.

(20) Niu, G.; Guo, X.; Wang, L. Review of recent progress in chemical stability of perovskite solar cells. *J. Mater. Chem. A* **2015**, *3*, 8970−8980.

(21) Tiep, N. H.; Ku, Z.; Fan, H. J. Recent Advances in Improving the Stability of Perovskite Solar Cells. *Adv. Energy Mater.* **2016**, *6*, 1501420.

(22) Stoumpos, C. C.; Soe, C. M. M.; Tsai, H.; Nie, W.; Blancon, J.-C.; Cao, D. H.; Liu, F.; Traoré, B.; Katan, C.; Even, J.; Mohite, A. D.; Kanatzidis, M. G. High Members of the 2D Ruddlesden-Popper Halide Perovskites: Synthesis, Optical Properties, and Solar Cells of $(CH_3(CH_2)_3NH_3)_2(CH_3NH_3)_4Pb_5I_{16}$. *Chem.* **2017**, *2*, 427−440.

(23) Grancini, G.; Roldan-Carmona, C.; Zimmermann, I.; Mosconi, E.; Lee, X.; Martineau, D.; Narbey, S.; Oswald, F.; De Angelis, F.; Graetzel, M.; Nazeeruddin, M. K. One-Year stable perovskite solar cells by 2D/3D interface engineering. *Nat. Commun.* **2017**, *8*, 15684−15691.

(24) Tsai, H.; Nie, W.; Blancon, J.-C.; Stoumpos, C. C.; Asadpour, R.; Harutyunyan, B.; Neukirch, A. J.; Verduzco, R.; Crochet, J. J.; Tretiak, S.; Pedesseau, L.; Even, J.; Alam, M. A.; Gupta, G.; Lou, J.; Ajayan, P. M.; Bedzyk, M. J.; Kanatzidis, M. G.; Mohite, A. D. High-efficiency two-dimensional Ruddlesden-Popper perovskite solar cells. *Nature* **2016**, *536*, 312−316.

(25) Wang, Z.; Lin, Q.; Chmiel, F. P.; Sakai, N.; Herz, L. M.; Snaith, H. J. Efficient ambient-air-stable solar cells with 2D−3D hetero-structured butylammonium-caesium-formamidinium lead halide perovskites. *Nat. Energy* **2017**, *2*, 17135−17144.

(26) Lee, J. W.; Dai, Z.; Han, T. H.; Choi, C.; Chang, S. Y.; Lee, S. J.; De Marco, N.; Zhao, H.; Sun, P.; Huang, Y.; Yang, Y. 2D perovskite stabilized phase-pure formamidinium perovskite solar cells. *Nat. Commun.* **2018**, *9*, 3021−3030.

(27) Thote, A.; Jeon, I.; Lee, J.-W.; Seo, S.; Lin, H.-S.; Yang, Y.; Daiguji, H.; Maruyama, S.; Matsuo, Y. Stable and Reproducible 2D/3D Formamidinium−Lead−Iodide Perovskite Solar Cells. *ACS Appl. Energy Mater.* **2019**, *2*, 2486−2493.

(28) Stoumpos, C. C.; Cao, D. H.; Clark, D. J.; Young, J.; Rondinelli, J. M.; Jang, J. I.; Hupp, J. T.; Kanatzidis, M. G. Ruddlesden−Popper Hybrid Lead Iodide Perovskite 2D Homologous Semiconductors. *Chem. Mater.* **2016**, *28*, 2852−2867.

(29) Calabrese, J.; Jones, N. L.; Harlow, R. L.; Herron, N.; Thorn, D. L.; Wang, Y. Preparation and Characterization of Layered Lead Halide Compounds. *J. Am. Chem. Soc.* **1991**, *113*, 2328−2330.

(30) Koh, T. M.; Shanmugam, V.; Guo, X.; Lim, S. S.; Filonik, O.; Herzig, E. M.; Müller-Buschbaum, P.; Swamy, V.; Chien, S. T.; Mhaisalkar, S. G.; Mathews, N. Enhancing moisture tolerance in efficient hybrid 3D/2D perovskite photovoltaics. *J. Mater. Chem. A* **2018**, *6*, 2122−2128.

(31) Wygant, B. R.; Ye, A. Z.; Dolocan, A.; Vu, Q.; Abbot, D. M.; Mullins, C. B. Probing the Degradation Chemistry and Enhanced

Stability of 2D Organolead Halide Perovskites. *J. Am. Chem. Soc.* **2019**, *141*, 18170−18181.

(32) Quan, L. N.; Yuan, M.; Comin, R.; Voznyy, O.; Beauregard, E. M.; Hoogland, S.; Buin, A.; Kirmani, A. R.; Zhao, K.; Amassian, A.; Kim, D. H.; Sargent, E. H. Ligand-Stabilized Reduced-Dimensionality Perovskites. *J. Am. Chem. Soc.* **2016**, *138*, 2649−2655.

(33) Proppe, A. H.; Wei, M.; Chen, B.; Quintero-Bermudez, R.; Kelley, S. O.; Sargent, E. H. Photochemically Cross-Linked Quantum Well Ligands for 2D/3D Perovskite Photovoltaics with Improved Photovoltage and Stability. *J. Am. Chem. Soc.* **2019**, *141*, 14180−14189.

(34) Smith, I. C.; Hoke, E. T.; Solis-Ibarra, D.; McGehee, M. D.; Karunadasa, H. I. A layered Hybrid Perovskite Solar-cell Absorber with Enhanced Moisture Stability. *Angew. Chem.* **2014**, *126*, 11414−11417.

(35) Wygant, B. R.; Geberth, G. T.; Ye, A. Z.; Dolocan, A.; Cotton, D. E.; Roberts, S. T.; Vanden Bout, D. A.; Mullins, C. B. Moisture-Driven Formation and Growth of Quasi-2-D Organolead Halide Perovskite Crystallites. *ACS Appl. Energy Mater.* **2020**, *3*, 6280−6290.

(36) Zhao, C.; Tian, W.; Sun, Q.; Yin, Z.; Leng, J.; Wang, S.; Liu, J.; Wu, K.; Jin, S. Trap-Enabled Long-Distance Carrier Transport in Perovskite Quantum Wells. *J. Am. Chem. Soc.* **2020**, *142*, 15091−15097.

(37) Song, Z.; Shrestha, N.; Watthage, S. C.; Liyanage, G. K.; Almutawah, Z. S.; Ahangharnejhad, R. H.; Phillips, A. B.; Ellingson, R. J.; Heben, M. J. Impact of Moisture on Photoexcited Charge Carrier Dynamics in Methylammonium Lead Halide Perovskites. *J. Phys. Chem. Lett.* **2018**, *9*, 6312−6320.

(38) Leguy, A. M. A.; Hu, Y.; Campoy-Quiles, M.; Alonso, M. I.; Weber, O. J.; Azarhoosh, P.; van Schilfgaarde, M.; Weller, M. T.; Bein, T.; Nelson, J.; Docampo, P.; Barnes, P. R. F. Reversible Hydration of $CH_3NH_3PbI_3$ in Films, Single Crystals, and Solar Cells. *Chem. Mater.* **2015**, *27*, 3397−3407.

(39) Spanopoulos, I.; Hadar, I.; Ke, W.; Tu, Q.; Chen, M.; Tsai, H.; He, Y.; Shekhawat, G.; Dravid, V. P.; Wasielewski, M. R.; Mohite, A. D.; Stoumpos, C. C.; Kanatzidis, M. G. Uniaxial Expansion of the 2D Ruddlesden-Popper Perovskite Family for Improved Environmental Stability. *J. Am. Chem. Soc.* **2019**, *141*, 5518−5534.

(40) Lee, J.-W.; Kim, D.-H.; Kim, H.-S.; Seo, S.-W.; Cho, S. M.; Park, N.-G. Formamidinium and Cesium Hybridization for Photo-and Moisture-Stable Perovskite Solar Cell. *Adv. Energy Mater.* **2015**, *5*, 1501310.

(41) Shi, L.; Bucknall, M. P.; Young, T. L.; Zhang, M.; Hu, L.; Bing, J.; Lee, D. S.; Kim, J.; Wu, T.; Takamure, N.; McKenzie, D. R.; Huang, S.; Green, M. A.; Ho-Baillie, A. W. Y. Gas chromatography-mass spectrometry analyses of encapsulated stable perovskite solar cells. *Science* **2020**, *368*, 1328−1335.

(42) Yang, J.; Siempelkamp, B. D.; Liu, D.; Kelly, T. L. Investigation of $CH_3NH_3PbI_3$ Degradation Rates and Mechanisms in Controlled Humidity Environments Using in Situ Techniques. *ACS Nano* **2015**, *9*, 1955−1963.

(43) Yan, L.; Niu, H. J.; Duong, G. V.; Suchomel, M. R.; Bacsa, J.; Chalker, P. R.; Hadermann, J.; van Tendeloo, G.; Rosseinsky, M. J. Cation ordering within the perovskite block of a six-layer Ruddlesden-Popper oxide from layer-by-layer growth − artificial interfaces in complex unit cells. *Chem. Sci.* **2011**, *2*, 261−272.

(44) Wu, X.; Trinh, M. T.; Niesner, D.; Zhu, H.; Norman, Z.; Owen, J. S.; Yaffe, O.; Kudisch, B. J.; Zhu, X. Y. Trap states in lead iodide perovskites. *J. Am. Chem. Soc.* **2015**, *137*, 2089−2096.

(45) Liu, J.; Leng, J.; Wu, K.; Zhang, J.; Jin, S. Observation of Internal Photoinduced Electron and Hole Separation in Hybrid Two-Dimensional Perovskite Films. *J. Am. Chem. Soc.* **2017**, *139*, 1432−1435.

(46) Frost, J. M.; Butler, K. T.; Brivio, F.; Hendon, C. H.; van Schilfgaarde, M.; Walsh, A. Atomistic origins of high-performance in hybrid halide perovskite solar cells. *Nano Lett.* **2014**, *14*, 2584−2590.

(47) Patel, J. B.; Milot, R. L.; Wright, A. D.; Herz, L. M.; Johnston, M. B. Formation Dynamics of $CH_3NH_3PbI_3$ Perovskite Following Two-Step Layer Deposition. *J. Phys. Chem. Lett.* **2016**, *7*, 96−102.